Open Research Online

The Open University's repository of research publications
and other research outputs

Data assimilation of three mars years of thermal emission spectrometer observations: Large-scale transient and stationary waves

Conference or Workshop Item

For guidance on citations see FAQs.

oro.open.ac.uk

DATA ASSIMILATION OF THREE MARS YEARS OF THERMAL EMISSION SPECTROMETER OBSERVATIONS: LARGE-SCALE TRANSIENT AND STATIONARY WAVES.

S. R. Lewis[1], L. Montabone[1], P. L. Read[2], P. Rogberg[2], R. J. Wilson[3] and M. D. Smith[4], [1]Department of Physics & Astronomy, The Open University, Walton Hall, Milton Keynes MK7 6AA, UK (S.R.Lewis@open.ac.uk), [2]Atmospheric, Oceanic & Planetary Physics, Department of Physics, University of Oxford, Clarendon Laboratory, Parks Road, Oxford OX1 3PU, UK, [3]Geophysical Fluid Dynamics Laboratory, National Oceanic and Atmospheric Administration, Princeton, New Jersey, USA, [4]NASA Goddard Space Flight Center, Greenbelt, Maryland, USA.

Introduction: Large-scale traveling and stationary planetary waves are diagnosed from an analysis of profiles retrieved from the Thermal Emission Spectrometer (TES) [1] aboard the Mars Global Surveyor (MGS) spacecraft during its scientific mapping phase. The analysis was conducted by assimilating the TES temperature profile and total dust opacity retrievals [2] into a pseudo-spectral Mars general circulation model to produce a full, physically self-consistent record of all atmospheric variables stored at an interval of two hours over the entire MGS mapping phase. The data cover a period of about three Mars years, corresponding to the interval 1999–2004 on Earth. These include the year which contained the 2001 global dust storm [3] and two years of more moderate dust activity, although large regional storms occurred during southern hemisphere summer in both years and there was considerable atmospheric variability between all three years [4].

We focus on the planetary wave activity, both traveling and stationary large-scale waves, in the assimilated record. Data assimilation is a particularly useful technique for the analysis of transient wave behaviour since it is capable of producing global, time-dependent atmospheric fields, which the assimilation scheme endeavours to make as consistent as possible with whatever observations are available. These atmospheric variables may be sampled from the model as often as desired, on a regular grid of points. If particular variables, or regions of the atmosphere, are not observed directly, the model will at least ensure that they are consistent with the laws of physics incorporated within its framework.

A complex climatology of transient waves is revealed, modulated by the large-scale topography and surface thermal properties, the time of year and, crucially, the amount of dust suspended in the atmosphere. Some individual case studies show the temporal and spatial structures of the waves in the assimilation record, although the large data set has by no means been fully explored. Companion papers discuss the thermal atmospheric tides [5] and the processes associated with the initiation of dust storms [6] from the same assimilated analysis. Output from the same assimilation has also been used to identify potential deficiencies in the model, such as the lack of water ice clouds [7].

Data Assimilation: The data have been analysed by assimilation into a pseudo-spectral Mars general circulation model [8], making use of a sequential procedure known as the analysis correction scheme [9], a form of the successive corrections method which has proved simple and robust in trial studies with artificial data under Martian conditions [10, 11]. The entire period has been assimilated, with varying model parameters, at a default model triangular spectral truncation at a total wavenumber 31 (T31), with non-linear products evaluated on a 96×48 dynamical horizontal grid (physical processes are evaluated on a reduced 72×36 grid) and using a stretched vertical grid on 25 sigma surfaces up to about 100 km altitude. Periods of the dataset have been re-analysed with a high horizontal resolution model, truncated at total wavenumber 85 (T85), with a 256×128 dynamical grid, in order to test sensitivity to model resolution and a model with T170 resolution (a 512×256 dynamical grid) has also been used.

Assimilation of the TES data using this technique during the MGS aerobraking hiatus has been described [12], as has an analysis of the thermal tidal behaviour throughout the MGS mapping phase [13]. The mapping phase assimilation has been validated by a cross-comparison of model temperature profiles sampled at the same time and place as profiles obtained by radio occultation, also using the MGS spacecraft [14]. The results of this assimilation procedure are further validated in this paper by comparing the planetary waves in the assimilation with those from direct synoptic mapping analyses of the TES retrievals.

Assimilated data is available over more than three Mars years. For reference, the Mars Years (MY) are numbered here following the scheme of [15]. The assimilation includes the aerobraking hiatus period (MY23, L_S=190°–260°), during which time the orbital period was being reduced from 45 to 24 hours and the configuration was more difficult for atmospheric assimilation [12]. Following this, data are available, with only some short breaks in coverage, throughout almost three Mars Years of 2-hour period, mapping phase orbits (MY24, L_S=141° to MY27, L_S=72°).

Transient Waves: The assimilated model analysis have been compared with direct synoptic mapping analyses of TES temperatures [16, 17]. A very similar pattern of waves is revealed, where the techniques can be directly compared in the temperature field, but the assimilation permits the analysis of fields other than those measured directly, such as surface pressure.

The Hovmoller diagrams in Figures 1 and 2 show transient temperature on the 50Pa pressure surface (~25km altitude) and transient pressure, corrected to the Mars reference datum to remove topographic signals. Both variables are shown at 62.5°N over the entire northern hemisphere winter period, L_S=180°–360°, of MY 24, the first year in the reanalysis period. The temperature and pressure have been time-filtered to remove tides and quasi-stationary features.

A section of Figure 1 can be compared to the more direct analysis of the temperature observations in [18, Figure 2] and confirms that the assimilation is consistent with the temperature observations in this region of the atmosphere.

Transient waves can be seen to propagate eastwards in both diagrams. These waves have low zonal wavenumbers, primarily 1–3, with wavenumber 1 dominating throughout much of this period. Of interest is the period around L_S=220°–260°, when the atmospheric temperature shows a strong, long period wavenumber 1 signal (equivalent to a wobble in the polar vortex) which is detached from the weaker, shorter period waves seen near the surface in the pressure signal. A modulation from these waves can still be seen in the temperature signal. At other times the waves are broadly coherent over this altitude range.

It is also notable that the waves near the surface are stronger after the autumn equinox and before the spring equinox, whereas the 50Pa temperature signal peaks around winter solstice. This solsticial pause in the near-surface waves is seen to recur in all three years analysed. In Figure 2, the peaks in the surface pressure wave activity coincide with regional dust storms in the northern hemisphere and with enhanced zonal wavenumber 3 activity.
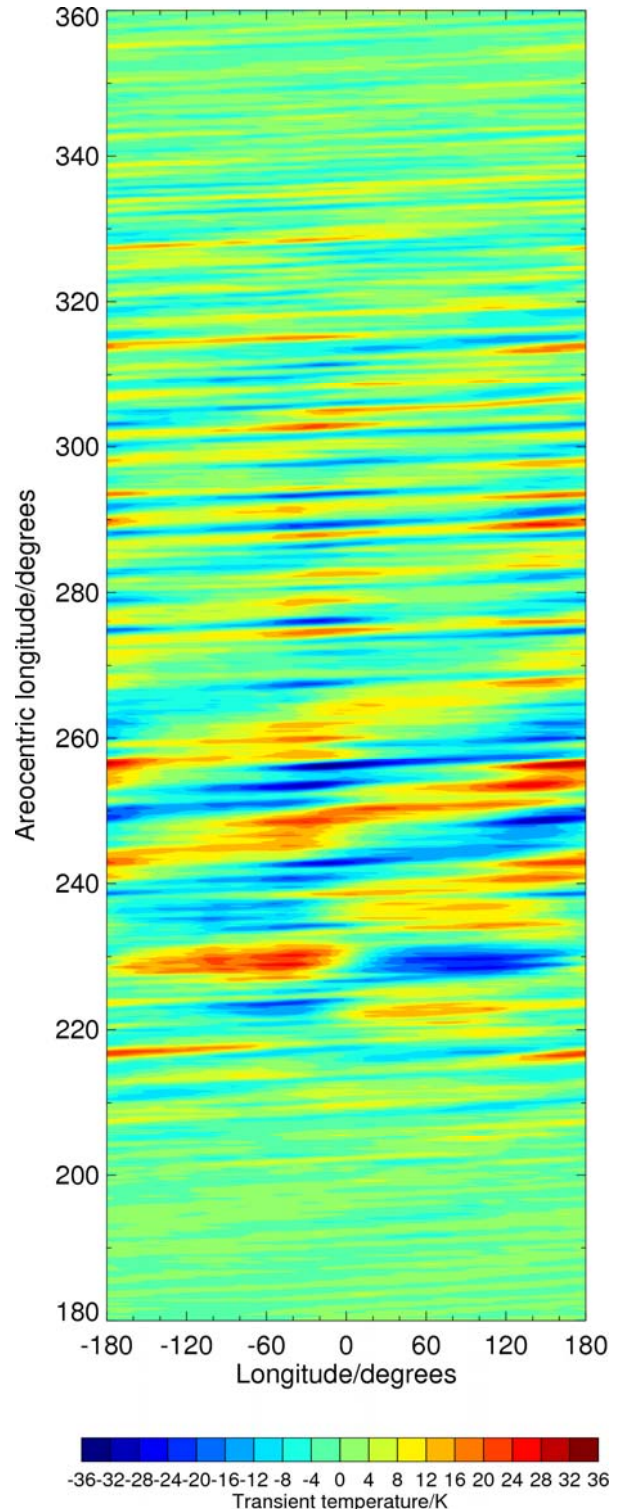

Figure 1: Transient temperature on the 50 Pa pressure surface (~25 km altitude) at 62.5°N over the period, LS=180°–360°, of MY 24.
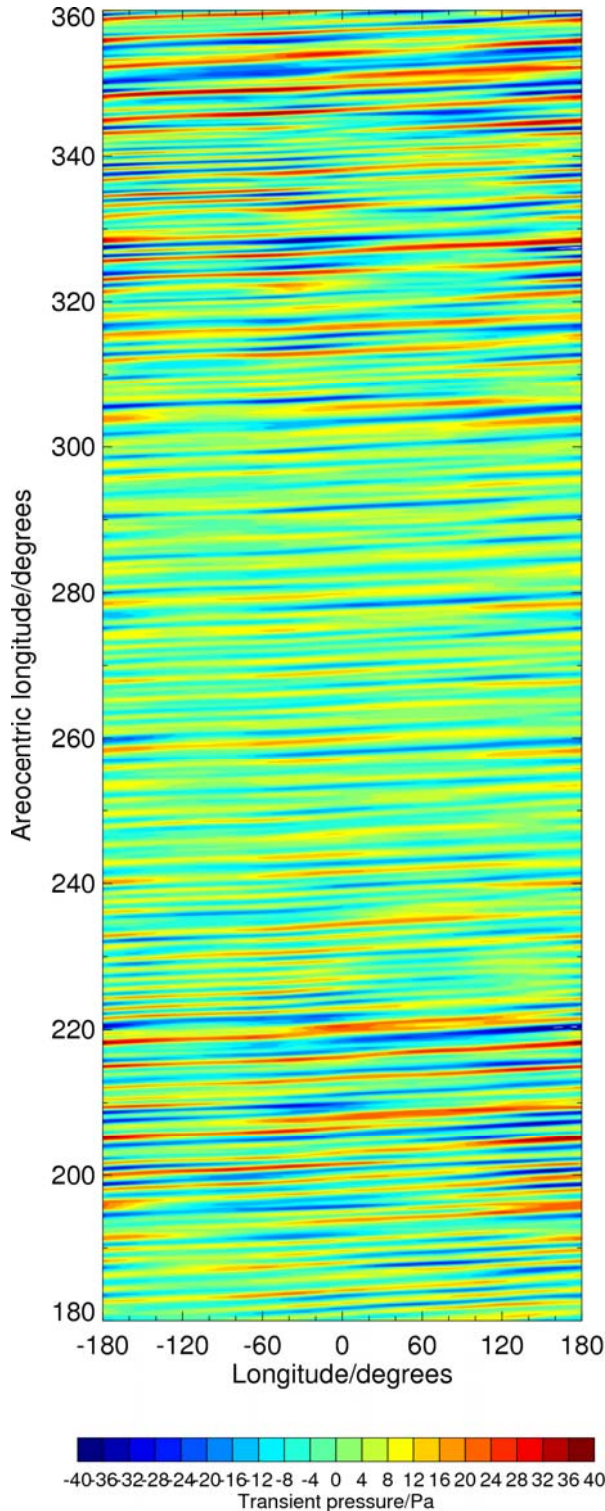
Figure 2: Transient pressure, corrected to the Mars reference datum to remove topographic signals at 62.5°N over the period, L$_S$=180°–360°, of MY 24.

Figure 3 illustrates the longitudinal mean of the root-mean-square meridional wind variability on the 400 Pa pressure surface (roughly 4 km above the mean surface), as a function of latitude and time of year. This clearly shows regions where the transient wave activity is large, notably in the winter hemisphere, but peaking just after autumn equinox and again before spring equinox, with a secondary minimum around winter solstice in each year and hemisphere. There is also transient wave activity in the southern hemisphere, but it is much weaker than that seen in the northern hemisphere. There is evidence of interannual variability in the strength of the transient waves, especially evident in the weaker waves seen around the time of the global dust storm from $L_S = 185°$ onwards in MY25.
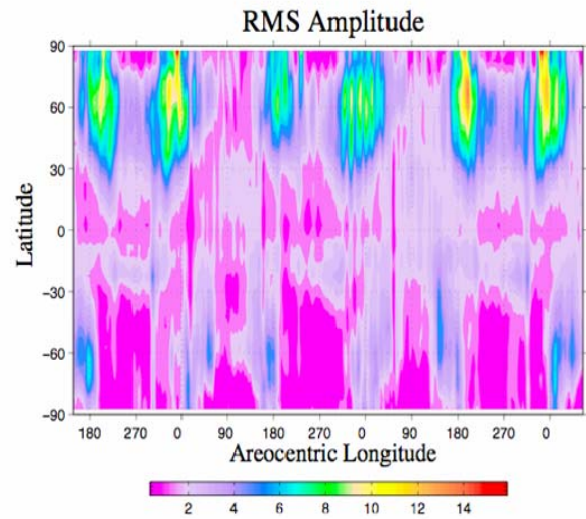
Figure 3: Root-mean-square amplitude of the variability of the meridional velocity (m/s) on the 400 Pa pressure surface as a function of latitude throughout the MY24, L$_S$=141° to MY27, L$_S$=72° period.

The regular sampling of the assimilated model data permits a straightforward Fourier analysis in longitude and time to identify zonal wavenumbers and their associated periods; generally longer periods of 6–8 days are associated with the zonal wavenumber 1 wave, whereas zonal wavenumbers 2 and 3 show significant amplitudes at shorter periods of 2–4 days. These three low zonal wavenumber modes tend to dominate all higher wavenumbers in the reanalysis record.
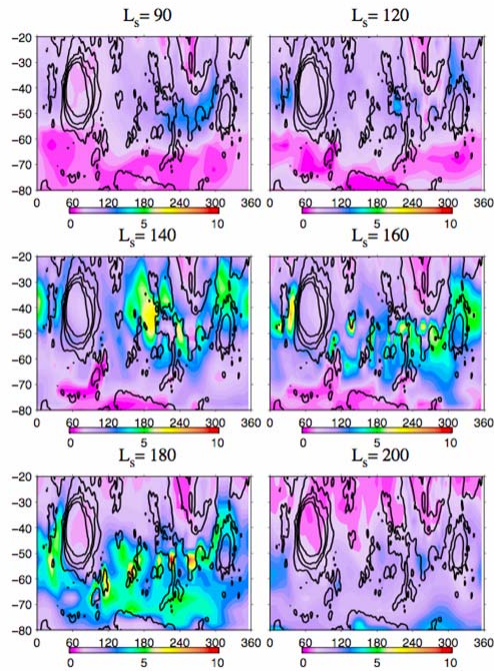
Figure 4: Root-mean-square variability of the meridional velocity (m/s) on the 400 Pa pressure surface in the southern hemisphere shown at intervals throughout the southern hemisphere winter of MY26. The solid contours show the topography for reference. Axes are latitude in degrees North and longitude in degrees East.

Figure 4 shows the presence of transient waves in the southern hemisphere, which are much more prominent in the assimilation than in independent model experiments. The waves are not uniform in longitude, but are broken up into a mid-latitude 'storm zone'. This is analogous to the stronger dual storm zones seen in the northern hemisphere of Mars [19] and the Earth. The strong topographic modulation of the transient waves is clear, with the Hellas basin breaking the symmetry of the weaker storm track, which moves southward as the season progresses and the seasonal polar ice cap retreats,.

Future Plans: The assimilation technique described here has proved robust and reliable for the entire TES/MGS period. Recent developments in data assimilation for the Earth, e.g. 4D-Var and the ensemble Kalman filter, should allow an improved analysis to be conducted, and this is the subject of current study. Data from Mars Climate Sounder on Mars Reconnaissance Orbiter are now providing a new oppor-

tunity to assimilate an extended atmospheric data set from a single orbiting satellite, a configuration that has already proved successful in the present study.

The results of these assimilations are intended to be accessible to the wider scientific community. This presents a practical challenge, since even the 2-hourly data set from a single, relatively moderate resolution model which has been run for three Mars years is several tens of gigabytes. One option is the production of climate statistics [20], but this results in the loss of detailed information describing transient atmospheric waves, such as those described in the present paper.

References: [1] Conrath B. J. et al. (2000) *JGR, 105 (E4),* 9509–9519. [2] Smith M. D. et al. (2001) *JGR, 106 (E10),* 23929–23945. [3] Smith M. D. et al. (2002) *Icarus, 157 (1),* 259–263. [4] Smith M. D. (2004) *Icarus, 167 (1),* 148–165. [5] Wilson R. J. et al. (2008) *3rd International Workshop on The Mars Atmosphere: Modeling and Observations.* [6] Montabone L. et al. (2008) *3rd International Workshop on The Mars Atmosphere: Modeling and Observations.* [7] Wilson R. J. et al. (2008) *GRL, 35,* L07202 [8] Forget F. et al. (1999) *JGR, 104 (E10),* 24155–24176. [9] Lorenc et al. (1991) *Quart. J. Roy. Meteorol. Soc., 117,* 59–89. [10] Lewis S. R. et al. (1996) *Planet. Space Sci., 44,* 1395–1409. [11] Lewis S. R. et al. (1997) *Adv. Space Res., 19,* 1267–1270. [12] Lewis et al. (2007) *Icarus, 192 (2),* 327–347. [13] Lewis S. R. and Barker P. (2005) *Adv. Space Res., 36,* 2162–2168. [14] Montabone L. et al. (2006) *Icarus, 185 (1),* 113–132. [15] Clancy R. T. et al. (2000) *JGR, 105 (E4),* 9553–9571. [16] Banfield D. et al. (2003) *Icarus, 161 (2),* 319–345. [17] Banfield D. et al. (2004) *Icarus, 170 (2),* 365–403. [18] Wilson R. J. et al. (2002) *GRL, 29 (14),* 1684. [19] Hollingsworth J. L. et al. (1996) *Nature, 380,* 413–416. [20] Lewis S. R. et al. (1999) *JGR, 104 (E10),* 24177–24194.